# AN INVESTIGATION OF THE FLUID DYNAMICS ASPECTS OF THIN LIQUID FILM PROTECTION SCHEMES FOR INERTIAL FUSION ENERGY REACTOR CHAMBERS

M. YODA,* S. I. ABDEL-KHALIK, and ARIES-IFE TEAM *Georgia Institute of Technology*
*G. W. Woodruff School of Mechanical Engineering, Atlanta, Georgia 30332-0405*

Received June 1, 2003
Accepted for Publication October 7, 2003

*Experimental and numerical studies of the fluid dynamics of thin liquid film wall protection systems have been conducted in support of the ARIES-IFE study. Both the porous "wetted wall" concept, involving low-speed injection through a porous wall normal to the surface, and the "forced film" concept, involving high-speed injection through slots tangential to the surface, have been examined. These initial studies focus upon the "preshot" feasibility of these concepts, between chamber clearing and the fusion event.*

*For the wetted wall, a three-dimensional level contour reconstruction method was used to track the evolution of the liquid film on downward-facing walls for different initial conditions and liquid properties with evaporation and condensation at the free surface. The effects of these parameters on the film dynamics, the free surface topology, the frequency of liquid drop formation and detachment, the minimum film thickness between explosions, and the equivalent diameter of detached drops have been analyzed. Initial experimental results are in reasonable agreement with the numerical predictions. Generalized nondimensional charts for identifying appropriate "design windows" for successful operation of the wetted wall protection concept have been developed. The results demonstrate that a minimum repetition rate is required to avoid liquid dripping into the reactor cavity and that a minimum injection velocity is required in order to maintain a minimum film thickness over the first wall.*

*For the forced film concept, experimental investigations of high-speed water films injected onto downward-facing flat and curved surfaces at angles of inclination up to 45 deg below the horizontal were conducted. Mean detachment length and the lateral extent of the film were measured for a wide range of liquid-solid contact angles at different values of the initial film thickness, liquid injection speed, and surface orientation. The results show that the film detaches earlier (i.e., farther upstream) for nonwetting surfaces and for flat (versus curved) surfaces. The nonwetting flat surface data are therefore used to establish a conservative "design window" for film detachment. Initial observations of film flow around cylindrical obstacles suggest that cylindrical dams are incompatible with forced films.*

**KEYWORDS:** *thin liquid protection, forced films, wetted wall*

## I. INTRODUCTION

In inertial fusion, the energy released from the exploding fuel pellets consists of energetic neutrons, photons, and charged particles that eventually dissipate their kinetic energies in the walls of the reactor chamber. The energy from the soft X rays and charged particles is deposited within an extremely thin surface layer, causing rapid surface heating of the reactor chamber first wall. These photon and ion irradiations may cause excessive wall erosion by numerous mechanisms, including evaporation, spallation and macroscopic erosion due to shock wave destruction, high thermal stresses, and intergranular pore explosion.

Numerous studies of the thermal-mechanical response of inertial fusion energy (IFE) reactor chamber first walls for different wall materials, target yields (i.e., wall loadings), repetition rates, and target designs (i.e., spectra) have been reported.[1–6] The results of these studies point to the need for a first wall protection scheme to

*E-mail: minami.yoda@me.gatech.edu

assure wall survival at practical cavity sizes. Several first wall protection schemes have been proposed over the last three decades, including the use of a thin sacrificial liquid film to protect the first wall from damaging radiation and thermal stresses. The Prometheus study,[7,8] which considered thin liquid film protection for both heavy-ion-beam and laser ignition, proposed using a film of liquid lead to protect the silicon carbide (SiC) first walls of the reactor chamber, a vertical cylinder with hemispherical end caps. The film was created using two different methods:

1. a "wetted wall" (a concept originally proposed by Los Alamos National Laboratory in 1972 (Ref. 9)), with a 0.5-mm-thick layer of liquid lead supplied through a porous SiC structure
2. a "forced film," where molten lead is injected at speeds exceeding 7 m/s through slots at the top of the chamber to create a few-millimeter-thick attached film over the upper chamber end cap.

The X rays produced by the exploding targets deposit their energy in the liquid lead, which prevents surface heating of the silicon carbide first wall. The ionic debris that arrives a few microseconds thereafter deposits its energy either in the lead vapor cloud produced by the X-ray energy deposition or in the remaining liquid film, thereby causing further evaporation. Recondensation of the vapor allows the energy deposited in the film to be recovered prior to the next target explosion, albeit over a longer time period, thereby limiting first wall heating and thermal stress. More recently, the feasibility of thin liquid layers attached to the first walls and controlled in part by electromagnetic forces has been explored as part of the APEX study on innovative concepts for magnetic fusion energy chamber technologies to attenuate neutrons and reduce surface heat flux.[10]

Prometheus envisioned injecting the forced film from a single point at the top (apex) of the reactor cavity. If the film is completely destroyed by the fusion event, however, and the film must be reestablished after each shot, this appears to be infeasible. For a cavity radius $R = 5$ m and a time between shots of 0.2 s (or a repetition rate of 5 Hz), the fluid must travel a distance of $\pi R$, over the upper hemispherical end cap, or 15.7 m, within 0.2 s, giving a minimum flow velocity of 78.5 m/s, which is a value well above speeds at which flowing liquids will erode the first wall. The only feasible method for implementing the forced film concept therefore appears to involve "tiling" the upper hemispherical end cap of the reactor cavity with multiple coolant injection and removal slots.

In 2001, the ARIES study began to develop design windows for IFE reactors using thin liquid film protection schemes based upon the Prometheus conceptual design. To this end, numerical and experimental studies have been performed by the Georgia Institute of Technology to examine the basic fluid dynamics of the wetted wall and forced film concepts. We have focused in these initial studies upon the "preshot" dynamics, or the evolution of these flows over the time period after the chamber is cleared until target ignition. The critical question for establishing the viability of these concepts is the following: Can a minimum film thickness be maintained to provide adequate protection during subsequent target explosions?

Among the most important fluid dynamics issues in thin liquid film protection are (a) preventing "dry patch" formation on the first wall; (b) preventing film detachment that may partially uncover the surface, thereby negating its effectiveness as a wall protectant; and (c) minimizing drop formation and detachment to avoid interference with target injection and beam propagation. In both the wetted wall and forced film concepts, film detachment and drop formation under the influence of gravity is most likely to occur on the downward-facing surfaces over the upper end cap of the reactor chamber. Moreover, this flow geometry—where a dense "heavy" liquid flows above a less dense "light" near-vacuum—may be susceptible to drop and even dry patch formation due to Rayleigh-Taylor instability (Refs. 11, 12, and 13, among others).

In the wetted wall concept, the appropriate model problem is that of a liquid film on a downward-facing flat surface at various angles of inclination with respect to the horizontal. Neglecting the first wall curvature is a reasonable assumption given that the radius of curvature for the Prometheus chamber upper end cap is ~5 m, or more than three orders of magnitude greater than film thicknesses of $O(10^{-3}$ m), and the flow velocities parallel to the wall are negligible. For the forced film, the large flow speeds tangential to the curved first wall generate a centrifugal force that stabilizes the film by driving the fluid outward against the wall. Forced film flows over both downward-facing flat and curved surfaces with a radius of curvature of 5 m were therefore investigated.

There have been several previous studies of the fluid dynamics and heat transfer of forced and free-falling laminar and turbulent liquid films on vertical and upward-facing inclined flat surfaces (Refs. 14 through 17, for example). Most of these studies have either focused upon the evolution and statistics of the free-surface waves on these films, or on modeling heat transfer in and minimum thickness of these flows. There has, however, been little work on liquid film flows on downward-facing solid surfaces, where a significant component of the gravitational force acts normal to the flow direction. We are aware of only one experimental study of forced film flow on a downward-facing surface, which reported that surface roughness had a major impact on detachment length for laminar water films in ambient air on flat acrylic surfaces up to 30 deg below the horizontal.[18]

A numerical investigation has therefore been conducted to examine the hydrodynamics of the wetted wall concept, which is modeled as a thin liquid film formed on

the downward-facing surface of a flat porous wall.[19–21] These simulations are being validated by experiments on water injected through a porous stainless steel surface. An experimental investigation is also being conducted to study the fluid dynamics of the forced film concept, modeled as a high-speed film of water injected tangentially onto the underside of both flat[22,23] and curved plates with a radius of 5 m. The objective of both efforts is to develop "design windows" to provide guidance for power plant designers on how important flow parameters (e.g., film thickness, liquid injection speed, surface orientation, and surface wettability) affect phenomena such as film detachment, drop formation and detachment, and minimum film thickness.

In this overview, Sec. II describes the numerical and experimental studies of the wetted wall concept, while Sec. III discusses the experiments on the forced film flow. Section IV summarizes the conclusions derived from these investigations and discusses the implications of these results for both of these thin liquid film protection concepts in IFE power plants.

## II. WETTED WALLS

In the numerical study of the wetted wall concept, a state-of-the-art level contour reconstruction technique has been developed and used to track the three-dimensional evolution of a thin liquid film with injection through a porous downward-facing wall with evaporation and condensation at the film free surface. The aim is to determine the effect of different design and operational parameters (initial film thickness, liquid injection velocity, mass flux at the film free surface, wall inclination angle, liquid properties, and surface disturbance amplitude and configuration) on the liquid film stability between explosions. Here, we report on the effects of these parameters on the transient, three-dimensional topology of the film free surface and the frequency of liquid drop formation and detachment. Formation and detachment of liquid drops from the downward-facing sections of the cavity surface may interfere with subsequent target and/or beam propagation and may render such a wall protection scheme unsuitable, at least for the upper sections of the cavity. Additionally, the effects of various parameters on the minimum film thickness prior to drop detachment are examined.

### II.A. Numerical Formulation

The numerical technique is based upon a finite difference/front tracking method originally developed for two- and three-dimensional isothermal multifluid flows.[24,25] One of the major advantages of this method is its ability to naturally and automatically handle interface merging and breakup in three-dimensional flows. A more detailed description of the numerical techniques is given by Shin.[25]

One set of transport equations, valid for both fluids (namely, the liquid injected through the porous wall and the cavity "gas"), is solved. This local, single-field formulation incorporates the effect of the interface in the equations as delta-function source terms, which act only at the interface.

The interface is advected in a Lagrangian fashion by integrating

$$\frac{d\mathbf{x}_f}{dt}\cdot\mathbf{n} = \mathbf{V}\cdot\mathbf{n} \ , \tag{1}$$

where

$\mathbf{x}_f = \mathbf{x}(s,t)$ = parameterization of the interface

$\mathbf{n}$ = unit normal to the interface

$\mathbf{V}$ = interface velocity vector.

In the absence of mass exchange (i.e., evaporation or condensation) at the gas-liquid interface, the interface velocity will be equal to the fluid velocity at the interface, or $\mathbf{V} = \mathbf{u}_f = \mathbf{u}(\mathbf{x}_f)$. On the other hand, when mass exchange takes place, the interface velocity components are given by

$$\frac{d\mathbf{x}_f}{dt} = \mathbf{u}_L + \frac{\dot{m}_f''}{\rho_L}\mathbf{n} \ , \tag{2}$$

where

$\mathbf{u}_L$ = heavier fluid (liquid) velocity at the interface

$\rho_L$ = liquid density

$\dot{m}_f''$ = mass flux from the gas to the liquid at the interface (positive for condensation and negative for evaporation).

Equation (2) specifies only the normal component of the interface motion; we assume that the interface and fluid at the interface have the same tangential velocity component.

The momentum equation is written for the entire flow field, and the forces due to surface tension are applied at the interface as body forces that act only at the interface. For the confined Rayleigh-Taylor instability simulation performed here, mass exchange at the interface is accounted for parametrically. We can therefore use a single nondimensional momentum equation for both fluids, without having to solve the energy equation. More importantly, by parametrically accounting for mass exchange at the interface, we can address all the relevant physical phenomena without restricting this analysis to specific target output spectra, chamber design, or fluid properties. Hence, we have accounted for the dominant nonisothermal effects, i.e., evaporation and condensation at the interface, by introducing a parametrically specified

interfacial mass flux $\dot{m}_f''$ as a source term in the conservation of mass and interface advection.

In nondimensionalizing the governing equations and boundary conditions, we define the length scale $l = \sqrt{\sigma/[g(\rho_L - \rho_G)]}$, the velocity scale $U_o = \sqrt{gl}$, the pressure scale $P_o = \rho_L U_o^2$, and the time scale $t_o = l/U_o$. Here, the subscript $L$ refers to the film liquid injected through the porous wall (heavy fluid), while the subscript $G$ refers to the low-pressure gas (vacuum) within the reactor cavity (light fluid). Thus, the governing nondimensional momentum equation can be expressed as

$$\frac{\partial \rho^+ \mathbf{u}}{\partial t} + \nabla\cdot(\rho^+ \mathbf{u}\mathbf{u}) = -\nabla p + \rho^+ \mathbf{g} + \frac{1}{\mathrm{Re}}\nabla\cdot\mu^+(\nabla\mathbf{u} + \nabla\mathbf{u}^T) + \int_A \frac{1}{\mathrm{We}}\kappa\mathbf{n}\delta(\mathbf{x} - \mathbf{x}_f)\,dA \ , \quad (3)$$

where

$$\frac{\rho_G}{\rho_L} = \rho^* \ ; \quad \frac{\mu_G}{\mu_L} = \mu^* \quad (4)$$

$$\rho^+ \equiv \rho(\mathbf{x},t)/\rho_L = 1 + (\rho^* - 1)I(\mathbf{x},t) \quad (5)$$

$$\mu^+ \equiv \mu(\mathbf{x},t)/\mu_L = 1 + (\mu^* - 1)I(\mathbf{x},t) \quad (6)$$

$$\mathrm{Re} = \frac{\rho_L U_o l}{\mu_L} \ ; \quad \mathrm{We} = \frac{\rho_L U_o^2 l}{\sigma} = \frac{\rho_L}{\rho_L - \rho_G} \ , \quad (7)$$

where

$p$ = pressure

$g$ = gravitational acceleration

$\sigma$ = surface tension coefficient

$\kappa$ = twice the mean interface curvature

$\delta(\mathbf{x} - \mathbf{x}_f)$ = three-dimensional delta function that is nonzero only when $\mathbf{x} = \mathbf{x}_f$.

The important nondimensional groups, the Reynolds and Weber numbers Re and We, respectively, are defined in Eq. (7). The integral term in Eq. (3) accounts for surface tension acting on the interface. In order to limit the scope of our study, we have assumed that the surface tension coefficient is constant, and thus, without loss of generality, we ignore tangential variations in $\sigma$ along the interface. We have also assumed the light fluid (IFE chamber cavity gas) to be inviscid, so the viscosity ratio defined in Eq. (4) is zero.

By including condensation and evaporation as a source term at the interface, the nondimensional conservation of mass can be written as

$$\nabla\cdot\rho^+\mathbf{u} = u\cdot\nabla\rho^+ + \frac{2(\rho^* - 1)}{\rho^* + 1}\int_A \dot{m}_f^*\delta(\mathbf{x} - \mathbf{x}_f)\,dA \ , \quad (8)$$

where the nondimensional mass flux is defined as $\dot{m}_f^* = \dot{m}_f''/(\rho_L U_o)$. Interface advection with finite phase change [Eq. (2)] can be expressed in nondimensional form as

$$\frac{d\mathbf{x}_f}{dt} = \mathbf{u}_L + \dot{m}_f^*\mathbf{n} \ . \quad (9)$$

The selected definitions for the length and velocity scales make the Weber number a function of only the density ratio $\rho_L/\rho_G$ [Eq. (7)]. Parametric calculations have been performed to quantify the effect of $\rho_L/\rho_G$ on the nondimensional drop detachment time, detached drop equivalent diameter, and liquid penetration distance prior to drop detachment.[19] These results show that for $\rho_L/\rho_G \geq 20$ (i.e., We $\leq 1.053$), the results are insensitive to further increases in $\rho_L/\rho_G$ (note that We $\to 1$ as $\rho_L/\rho_G \to \infty$). Obviously, $\rho_L/\rho_G \gg 20$ in IFE applications. Nevertheless, the results of the parametric calculations demonstrate that the effect of $\rho_L/\rho_G$ can be ignored for values above 20. The results presented here therefore use $\rho_L/\rho_G = 20$, or, equivalently, We = 1.053, to reduce the computing time required for the analyses.

### II.B. Boundary Conditions and Initial Perturbations

Figure 1 shows the calculation geometry and boundary conditions used to model horizontal, downward-facing surfaces with liquid injection through the surface.

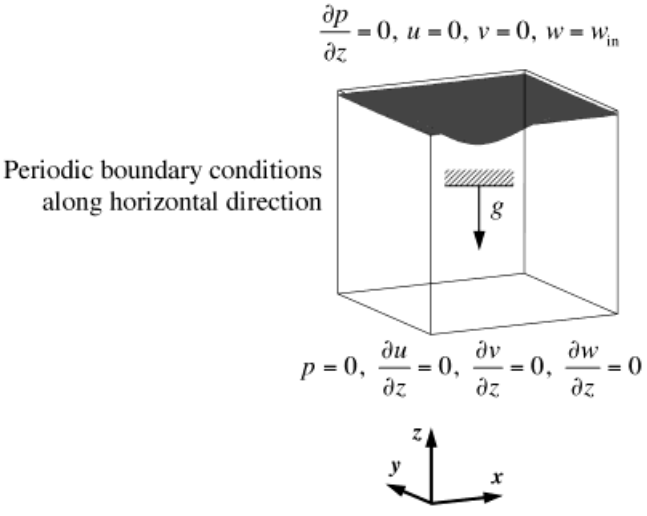


Fig. 1. Initial surface configuration and boundary conditions used to model horizontal downward-facing surfaces with liquid injection through the surface.

This corresponds to the uppermost point in the reactor cavity inner surface. The film is along the *x*-*y* plane of the flow, with the *z* direction oriented normal to the film pointing upward. Because of symmetry, periodic boundary conditions are used in the horizontal directions across the four vertical sides. Liquid is injected at a specified normal velocity $w_{in}$ at the upper solid boundary, while an open boundary condition is used at the bottom surface. The calculation geometry and boundary conditions used to model films on downward-facing inclined surfaces are shown in Fig. 2. Although the upper and lower surface boundary conditions are the same as those for the horizontal surface case, we impose Neumann conditions on the side boundaries for velocity and hydrostatic pressure conditions for the *x* and *y* directions. Gravity acts at an angle $\theta$ with respect to the vertical.

Clearly, in the relatively hostile environment following target explosion and chamber clearing, the initial film surface geometry would be highly uncertain. The effects of three different initial surface perturbation geometries, namely, the "sinusoidal," "saddle," and "random" perturbations (Fig. 3), on drop detachment time were considered at different mode numbers.[19] The results generally show that the saddle-type initial surface perturbation with a mode number of 1 produces the shortest drop detachment time, in agreement with previous studies of the Rayleigh-Taylor instability.[19] Grid convergence studies showed that simulations with nodal resolutions of ($50 \times 50 \times 50$) and ($100 \times 100 \times 100$) gave nearly identical drop detachment times. Therefore, all the results presented here were generated using the saddle-type perturbation with a mode number of unity over a $50 \times 50 \times 50$ mesh with a perturbation amplitude of half the initial surface thickness $z_o^*$. The large perturbation amplitude was chosen to represent the strongly disturbed film after target explosion and subsequent chamber clearing.

### II.C. Numerical Results

The effects of initial film thickness, liquid injection velocity, evaporation/condensation mass flux, and Reynolds number on the free-surface evolution and drop detachment time $t_d$ have been examined. Figure 4 shows four snapshots over time (with time increasing from left to right) of the film free surface for a thin film (nondimensional initial film thickness $z_o^* = 0.1$) and moderate injection velocity (normalized injection velocity $w_{in}^* = 0.01$) at nondimensional mass flux $\dot{m}_f^* = -0.005$ (evaporation) [left], 0.0 [center], and +0.01 (condensation) [right]. For lead at 800 K, these values correspond to an initial film thickness of 0.2 mm and injection velocity of 1.4 mm/s, giving a Reynolds number of 2000, and mass fluxes of −7.6, 0, and 15.2 kg/(m$^2$·s), respectively. The last snapshot for each case corresponds to the moment where a drop detaches; the nondimensional drop detachment time $\tau^* \equiv t_d/t_o$ is given at the bottom for all three cases. These results indicate that evaporation delays drop detachment (i.e., increases $\tau^*$), while condensation results in earlier detachment compared to the baseline case with $\dot{m}_f^* = 0$. The nondimensional detachment times $\tau^* = 31.35$, 27.69, and 25.90 correspond to detachment times $t_d = 0.46$, 0.41, and 0.38 s, respectively.

Similar calculations have been performed for a higher injection velocity of $w_{in}^* = 0.05$ (Fig. 5), while all other parameters remain unchanged. These results show that as $w_{in}$ increases, evaporation and condensation have relatively little impact upon $t_d$; $\tau^* = 25.69$, 25.13, and 25.74 for $\dot{m}_f^* = -0.005$ (evaporation) [left], 0.0 [center], and

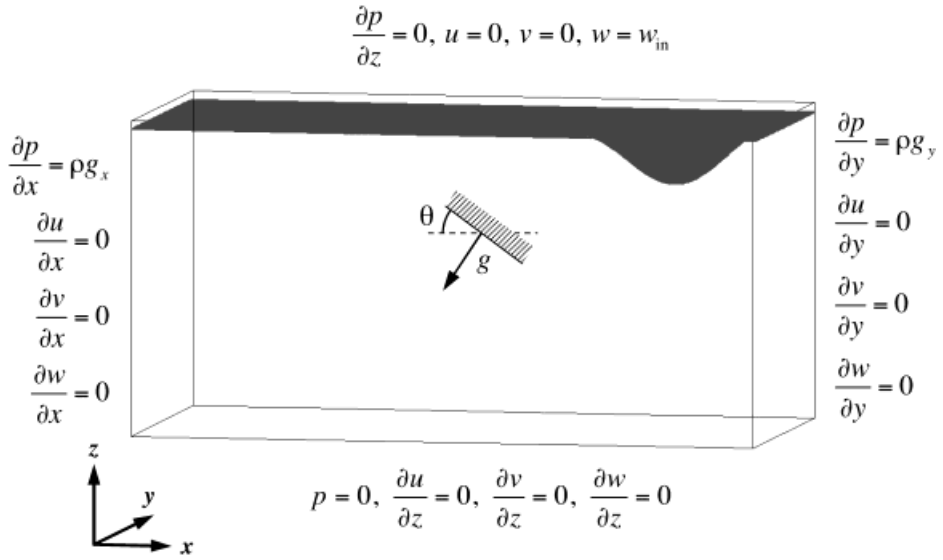


Fig. 2. Initial surface configuration and boundary conditions used to model inclined downward-facing surfaces with liquid injection through the surface.

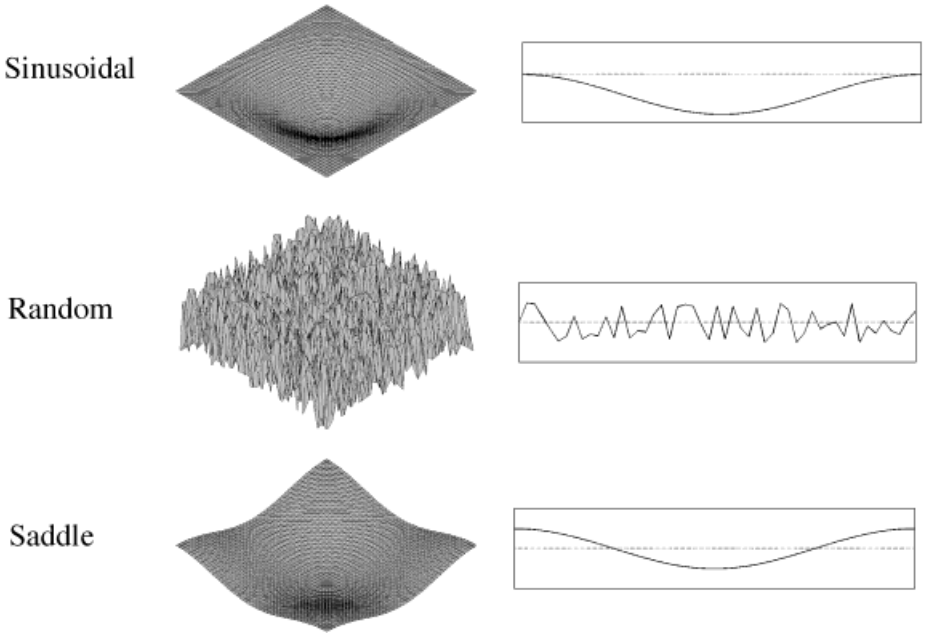


Fig. 3. Sketch of the three initial surface perturbation geometries (sinusoidal, random, and saddle) examined in this investigation.

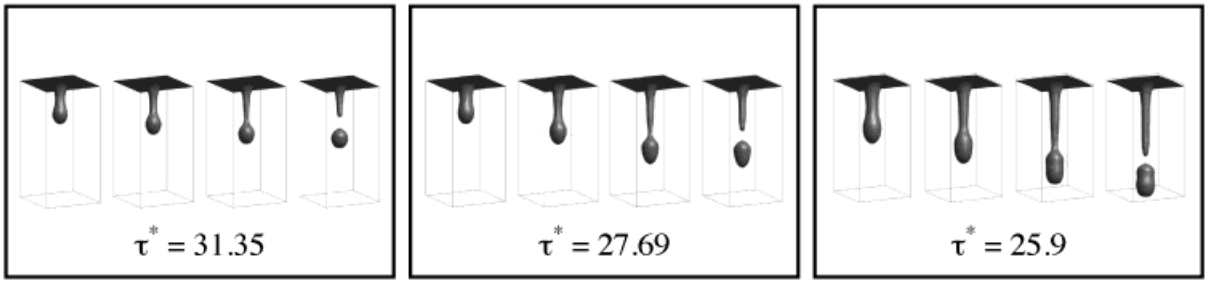


Fig. 4. Evolution of the film free surface over time (time progressing from left to right), with drop detachment occurring in the rightmost snapshot, showing the effect of evaporation/condensation at the interface on nondimensional drop detachment time $\tau^*$ for thin liquid films ($z_o^* = 0.1$) with moderate injection velocity ($w_{in}^* = 0.01$): $\dot{m}_f^* = -0.005$ (evaporation) [left], 0.0 [center], and 0.01 (condensation) [right]. In all cases, Re = 2000.

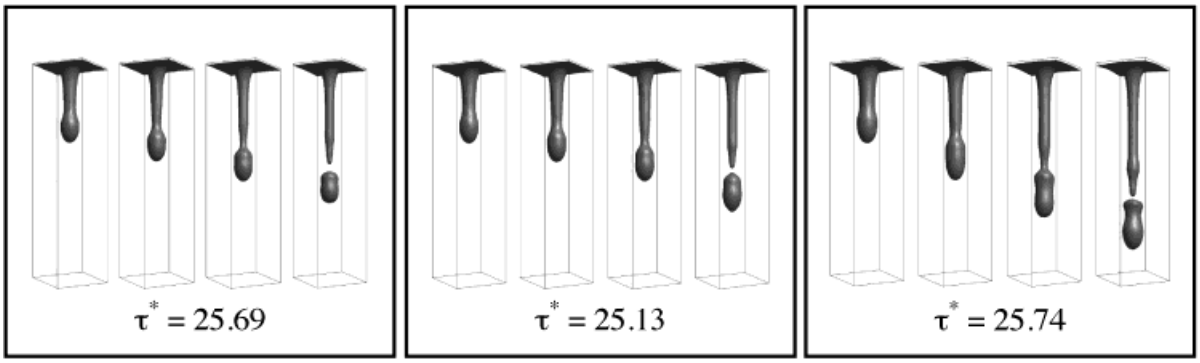


Fig. 5. Evolution of the film free surface showing the effect of evaporation/condensation at the interface on nondimensional drop detachment time $\tau^*$ for thin liquid films ($z_o^* = 0.1$) at a higher injection velocity ($w_{in}^* = 0.05$): $\dot{m}_f^* = -0.005$ (evaporation) [left], 0.0 [center], and 0.01 (condensation) [right]. In all cases, Re = 2000.

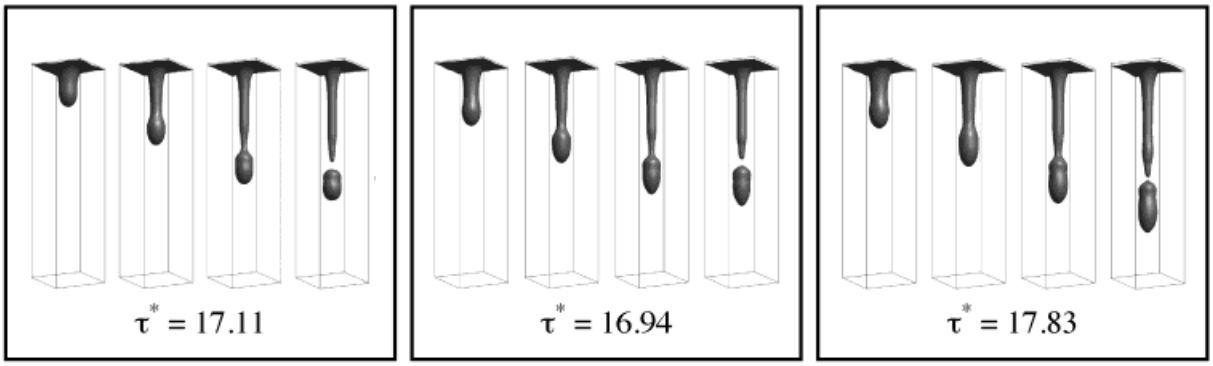


Fig. 6. Evolution of the film free surface (time progressing from left to right), with drop detachment occurring in the final snapshot, showing the effect of evaporation/condensation at the interface on nondimensional drop detachment time $\tau^*$ for thicker liquid films ($z_o^* = 0.1$) at a higher injection velocity ($w_{in}^* = 0.05$): $\dot{m}_f^* = -0.005$ (evaporation) [left], 0.0 [center], and 0.01 (condensation) [right]. In all cases, Re = 2000.

+0.01 (condensation) [right], respectively. Figure 6 shows similar calculations at a larger initial film thickness of $z_o^* = 0.5$, corresponding to an initial film thickness of ~1 mm for lead at 800 K (all other parameters are the same as those in Fig. 5). As expected, higher initial film thickness (with correspondingly larger initial disturbance amplitude) leads to smaller detachment time, with a reduction of nearly 30% compared with the cases shown in Fig. 5. For the thicker film, $\tau^* = 17.11$, 16.94, and 17.83 for $\dot{m}_f^* = -0.005$ (evaporation) [left], 0.0 [center], and +0.01 (condensation) [right], respectively. Nevertheless, the effects of mass transfer at the gas-liquid interface are relatively small for thicker films.

Generalized charts showing the nondimensional drop detachment time as a function of Reynolds number for different values of nondimensional mass flux $\dot{m}_f^*$ at the gas-liquid interface ranging from −0.005 to +0.02 are shown in Fig. 7 for three different values of initial film thickness and liquid injection velocity: (a) $z_o^* = 0.1$ and $w_{in}^* = 0.01$, (b) $z_o^* = 0.5$ and $w_{in}^* = 0.05$, and (c) $z_o^* = 0.5$ and $w_{in}^* = 0.01$. Figure 7a shows that detachment time decreases at a given Re as mass flux increases for thin films ($z_o^* = 0.1$). Figures 7b and 7c show that for relatively thick films ($z_o^* = 0.5$), the effect of all other parameters (including $\dot{m}_f^*$) on $\tau^*$ is relatively minor and that the detachment time is essentially constant for these cases.

Figure 7 can be used by the system designer to determine the expected drop detachment time, or frequency, for different design and operating conditions. Although the target explosion will generate numerous drops and clearing these drops, or "chamber clearing," is a major issue for liquid protection schemes, these simulations demonstrate that even an isothermal film will drip in the preshot interval between chamber clearing and the next target explosion. These drop detachment time results therefore imply that target explosions must occur at a frequency above a minimum repetition rate to minimize interference with target injection and ignition due to formation of preshot drops.

Figure 8 shows the evolution of the nondimensional minimum film thickness $\delta_{min}^* \equiv \delta_{min}/l$, where $\delta_{min}$ is the minimum film thickness observed over the entire film at any given time $t$, as a function of nondimensionalized time $t^* \equiv t/t_o \leq \tau^*$ at different Reynolds numbers ($50 \leq \mathrm{Re} \leq 2000$) for two cases: (a) $z_o^* = 0.1$ and $w_{in}^* = 0.05$ and (b) $z_o^* = 0.5$ and $w_{in}^* = 0.05$, both with no evaporation/condensation ($m_f^* = 0.0$). Figure 8 shows that $\delta_{min}^*$ gradually increases with injection and then decreases to a minimum value prior to drop separation. Figure 8a shows that for an initially thin film ($z_o^* = 0.1$), the minimum film thickness over the entire transient is actually higher than the initial value of $\delta_{min}^*$. The opposite is true for initially thick films ($z_o^* = 0.5$), as shown in Fig. 8b.

Recognizing the importance of this parameter to system designers, generalized nondimensional charts for $\delta_{min}^*$ as a function of Re for different evaporation and condensation rates have been developed for three different cases, as shown in Fig. 9: (a) $z_o^* = 0.5$ and $w_{in}^* = 0.05$, (b) $z_o^* = 0.1$ and $w_{in}^* = 0.01$, and (c) $z_o^* = 0.5$ and $w_{in}^* = 0.01$. These results suggest that the injection velocity must exceed a minimum value to keep the film thickness from decreasing below a designer-specified minimum value. Clearly, condensation at the liquid-gas interface reduces the minimum injection velocity required to prevent film dryout. Moreover, $\delta_{min}^*$ increases with $\dot{m}_f^*$ at a given Re for all three cases. Figure 9 can be used to determine the minimum film thickness for various design conditions and fluid properties. Alternatively, these generalized charts can be used to determine the necessary injection velocity corresponding to a desired value for the minimum film thickness and a given set of fluid properties and evaporation/condensation rates.

The nondimensional detached drop equivalent diameter $D^* \equiv D/l$ shown in Fig. 10 as a function of Re

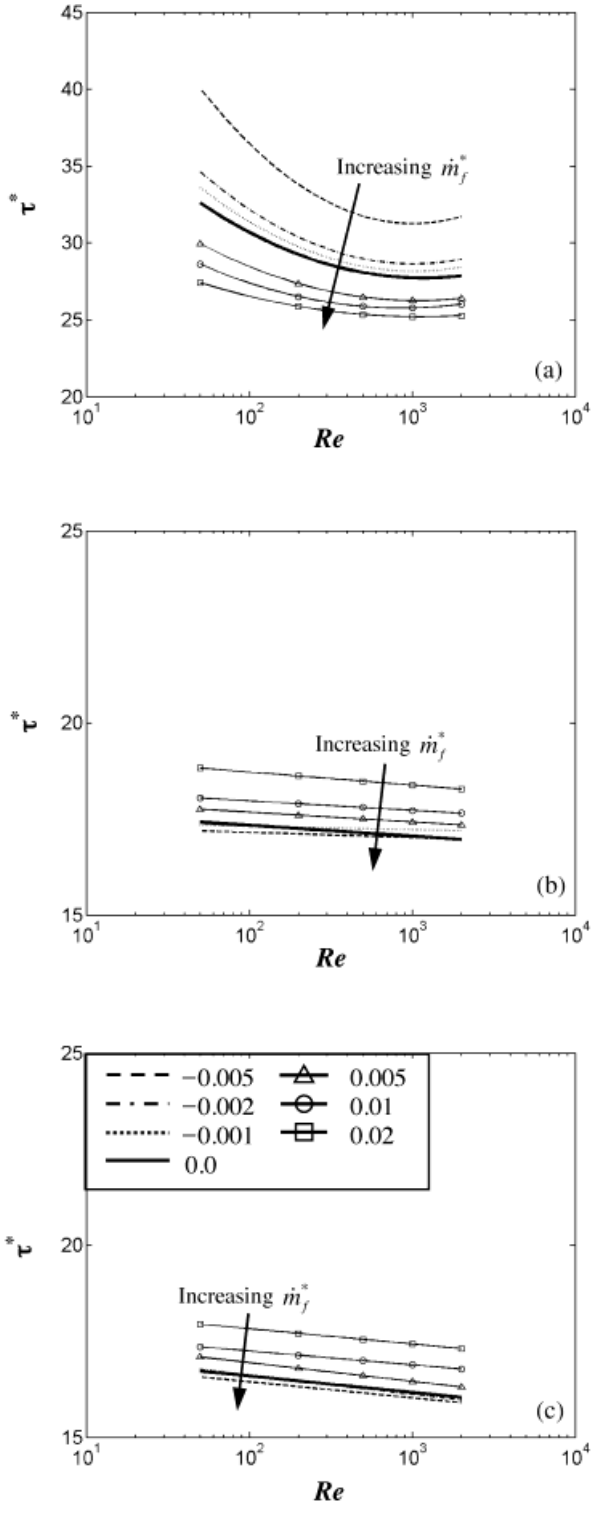


Fig. 7. Generalized charts for nondimensional drop detachment time $\tau^*$ as a function of Reynolds number Re [log scale] for different values of the normalized interfacial mass flux $\dot{m}_f^*$ (see legend). Three different initial film thicknesses and injection velocities are presented: (a) $z_o^*$ 0.1 and $w_{in}^* = 0.01$, (b) $z_o^* = 0.5$ and $w_{in}^* = 0.05$, and (c) $z_o^* = 0.5$ and $w_{in}^* = 0.01$. Note that the vertical scale of (a) is different from that for (b) and (c).

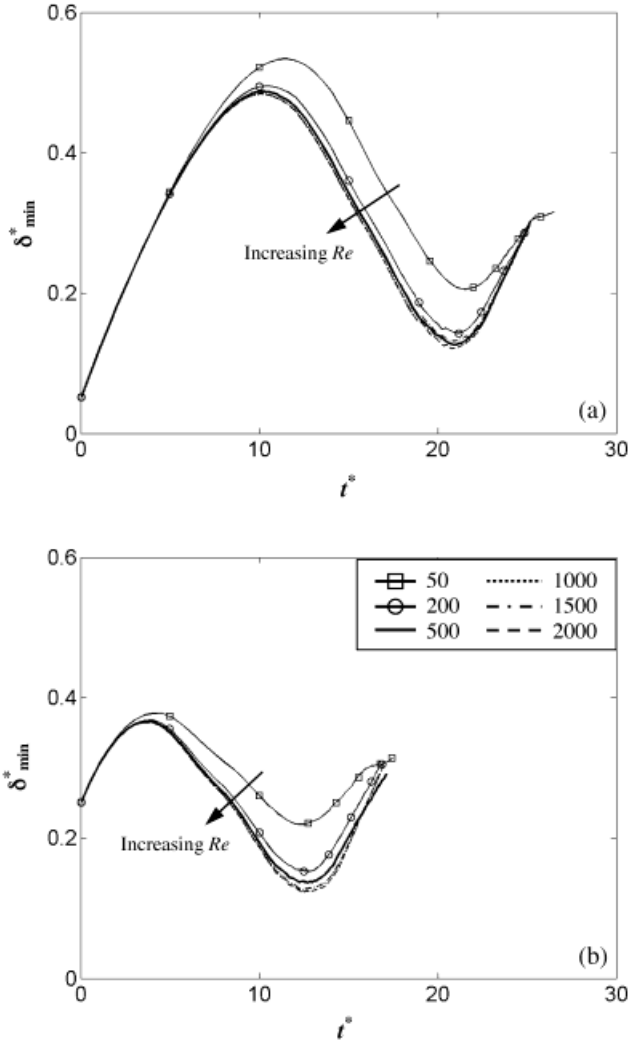


Fig. 8. Variation of the normalized minimum film thickness $\delta_{min}^*$ with nondimensionalized time $t^*$ at Reynolds numbers Re (see legend) for two cases: (a) $z_o^* = 0.1$ and $w_{in}^* = 0.05$ and (b) $z_o^* = 0.5$ and $w_{in}^* = 0.05$. In both cases, $m_f^* = 0.0$.

represents the diameter of a spherical drop $D$ with a volume equal to that of the liquid spike that separates from the liquid film at $t = t_d$. Figure 10 shows curves for seven different values of the nondimensional mass flux at the free surface ($-0.005 \le \dot{m}_f^* \le +0.02$). Graphs are presented for three different initial film thicknesses and injection velocities: (a) $z_o^* = 0.5$ and $w_{in}^* = 0.05$, (b) $z_o^* = 0.1$ and $w_{in}^* = 0.01$, and (c) $z_o^* = 0.5$ and $w_{in}^* = 0.01$. These results suggest that $D^*$ depends weakly on Re, increases with $\dot{m}_f^*$ at a given Re, and is strongly dependent upon the injection velocity and initial film thickness. Again, the results given in Fig. 10 allow the designer to estimate the size of detached drops from the liquid film for different design parameters and liquid properties.

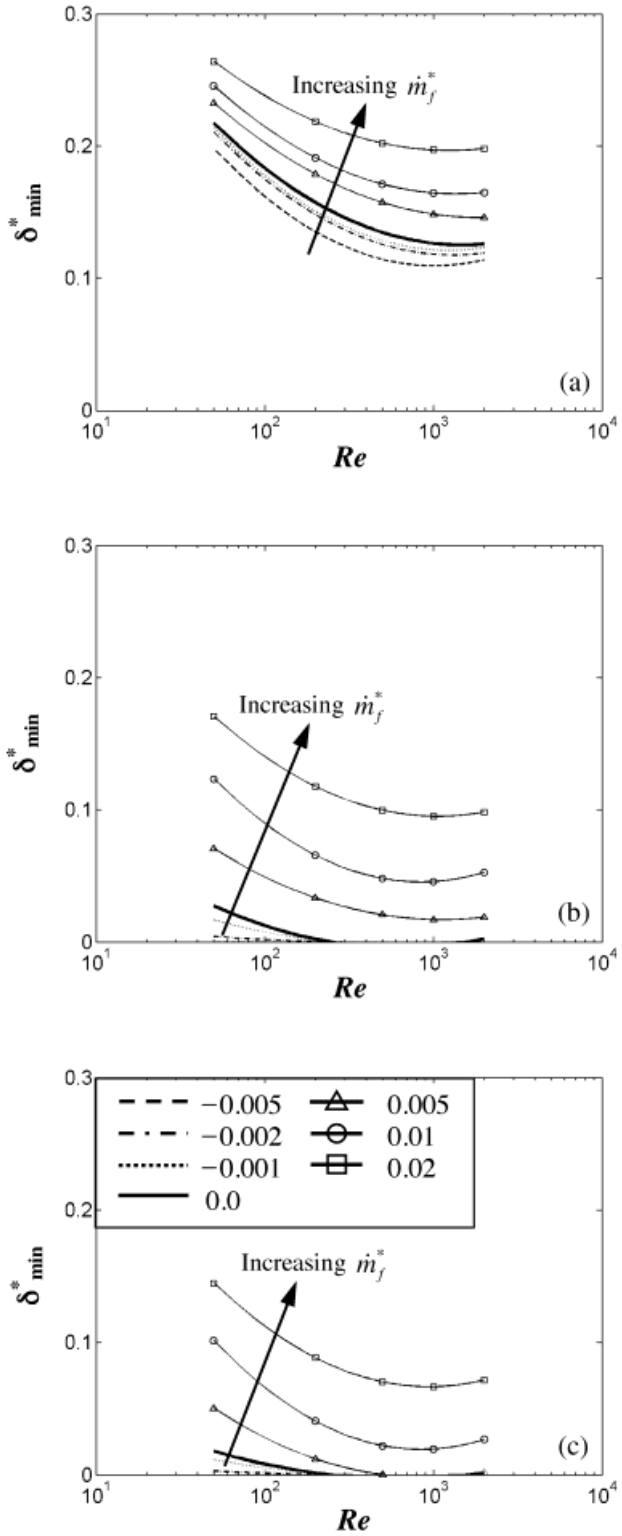


Fig. 9. Generalized charts for the normalized minimum film thickness $\delta^*_{min}$ as a function of Reynolds number Re [log scale] for different values of the normalized interfacial mass flux $\dot{m}_f^*$ (see legend). Three different initial film thicknesses and injection velocities are presented: (a) $z_o^* = 0.5$ and $w_{in}^* = 0.05$, (b) $z_o^* = 0.1$ and $w_{in}^* = 0.01$, and (c) $z_o^* = 0.5$ and $w_{in}^* = 0.01$.

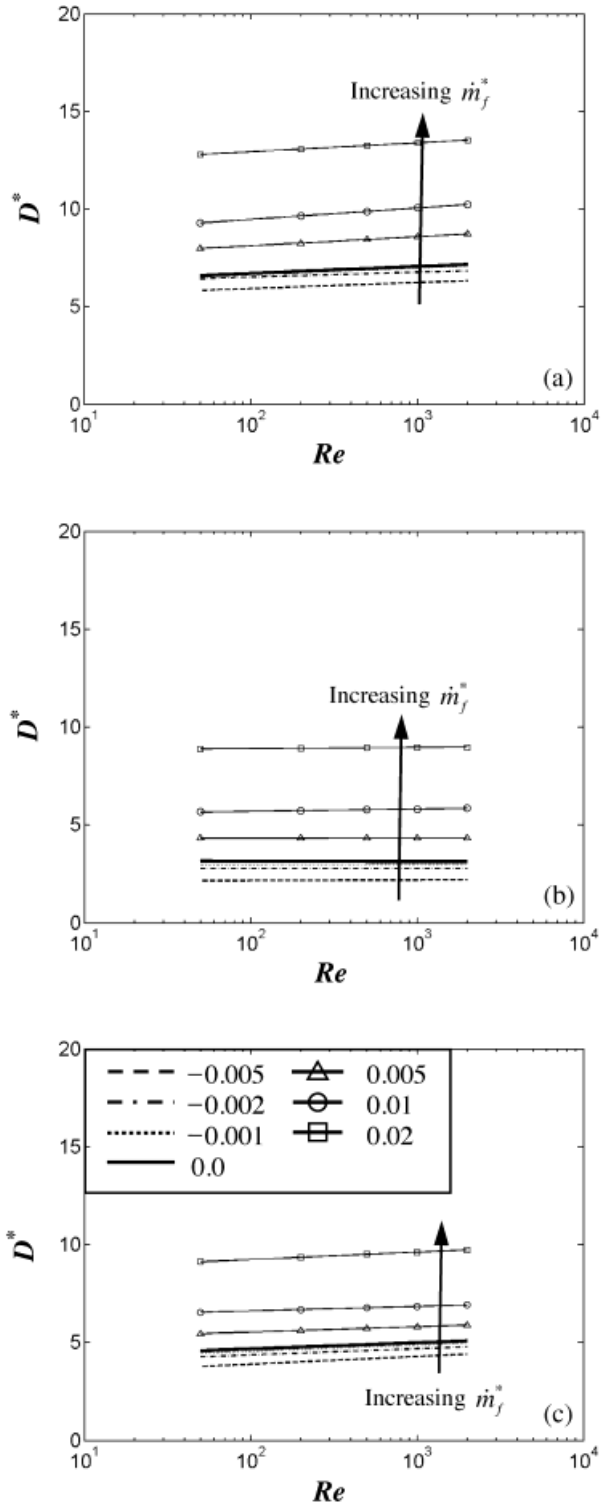


Fig. 10. Generalized charts for the normalized detached drop equivalent diameter $D^*$ as a function of Reynolds number Re [log scale] for different values of the normalized interfacial mass flux $\dot{m}_f^*$ (see legend). Three different initial film thicknesses and injection velocities are presented: (a) $z_o^* = 0.5$ and $w_{in}^* = 0.05$, (b) $z_o^* = 0.1$ and $w_{in}^* = 0.01$, and (c) $z_o^* = 0.5$ and $w_{in}^* = 0.01$.

TABLE I

The Length, Velocity, and Timescales ($l$, $U_o$, and $t_o$, respectively), Along with the Reynolds Number Re, for Different Fluids of Interest at Various Temperatures $T$

| | Water | | Lead | | Lithium | | Flibe | | |
|---|---|---|---|---|---|---|---|---|---|
| $T$ (K) | 293 | 323 | 700 | 800 | 523 | 723 | 773 | 873 | 973 |
| $l$ (mm) | 2.73 | 2.65 | 2.14 | 2.12 | 8.25 | 7.99 | 3.35 | 3.22 | 3.17 |
| $U_o$ (mm/s) | 163.5 | 161.2 | 144.7 | 144.2 | 284.4 | 280.0 | 181.4 | 177.8 | 176.4 |
| $t_o$ (ms) | 16.7 | 16.4 | 14.8 | 14.7 | 29.0 | 28.6 | 18.5 | 18.1 | 18.0 |
| Re | 445 | 771.2 | 1618 | 1831 | 1546 | 1775 | 81.80 | 130.8 | 195.3 |

### II.D. Experimental Validations

Table I gives values of the length, velocity, and timescales, along with the Re for several fluids at different temperatures. Table I shows that Re $\approx$ 500 for water at 300 K, suggesting that water can be used as a simulant fluid for a number of candidate IFE reactor coolants. Experiments using water as the working fluid can therefore provide useful data to validate the results given in Sec. II.C. An experimental recirculating test facility has been constructed where water supplied by a constant-head tank flows continuously through a porous stainless steel rectangular plate (nominal dimensions $12 \times 18$ cm) at an adjustable orientation angle $\theta$ with respect to the horizontal.[20] Different plate porosities and tank levels are used to vary the film thickness and injection velocity $w_{in}$.

Typical results showing the evolution of a liquid water drop from a horizontal porous surface ($\theta = 0$ deg) at $w_{in} = 10$ mm/s are shown in Fig. 11. Initial data for the drop detachment time at $\theta = 0$ deg and $w_{in} = 2.4$ mm/s over 40 different drops give a mean drop detachment time $t_d = 0.39$ s, with a standard deviation $\pm 0.04$ s, and a mean detached equivalent drop diameter $\bar{D} = 5.79 \pm 0.77$ mm. Based on an estimated film thickness of 1.0 mm, these results compare well with the model predictions of $t_d = 0.36$ s and $D = 5.5$ mm. We are currently developing techniques to accurately and nonintrusively measure the initial film thickness using optical techniques to obtain more accurate comparisons with the numerical simulations.

## III. FORCED FILMS

This section deals with the fluid dynamics aspects of the forced thin liquid film wall protection scheme, where the liquid is tangentially injected along the first wall surface. As discussed previously, avoiding the formation of dry patches is a major issue for effective thin film protection. For dry patch formation in a forced film flow driven by forces tangential to the surface (e.g., thermocapillary and surface forces), recent results using minimum total energy criteria[17] show that for an isothermal liquid film flowing down a vertical adiabatic wall, the minimum film thickness required to rewet any dry patch $\delta_{min}$ is given by the empirical relation

$$\Delta_{min} \equiv \delta_{min}\left(\frac{15\mu_L^2\sigma}{\rho_L^3 g^2}\right) = (1 - \cos\theta_o)^{0.22} \quad , \qquad (10)$$

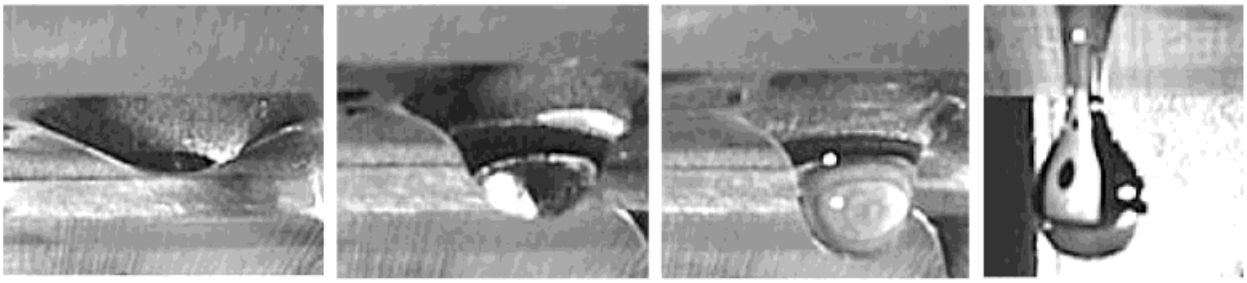


Fig. 11. Typical images showing the evolution of a film of water on the underside of a horizontal porous plate at times $t = 0.05$, 0.1, 0.15, and 0.2 s for an injection velocity $w_{in} = 10$ mm/s.

where $\Delta_{min}$ is the nondimensional minimum film thickness and $\theta_o$ is the contact angle of the liquid on the wall. The minimum mass flow rate per unit perimeter required to rewet any dry patch $\gamma_{min}$ is then

$$\Gamma_{min} \equiv \gamma_{min}\left(\frac{g}{\rho_L \mu_L \sigma^3}\right)^{0.2} = 0.67\Delta_{min}^{2.83} + 0.26\Delta_{min}^{9.51} , \quad (11)$$

where $\Gamma_{min}$ is the nondimensional flow rate. Application of Eqs. (10) and (11) shows that $\delta_{min} < 1$ mm and the minimum film average speed required for a stable fully wetted liquid film $<1$ m/s for most IFE coolants of interest and water with 0 deg $\leq \theta_o \leq$ 90 deg. The minimum required film thickness scales as $g^2$, while the minimum required film speed is weakly dependent on gravity, scaling as $g^{-0.2}$. Dry patch formation and rewetting in forced film flow over a vertical wall is hence the "worst case" from a purely hydrodynamic viewpoint at the expected liquid film velocities in IFE systems (which are much greater than 1 m/s) since the streamwise component of gravity is greatest for this orientation. Based on these results, our efforts have focused on the detachment of thin liquid films flowing along downward-facing surfaces where gravitational and surface tension effects become dominant.

Turbulent films on downward-facing surfaces were experimentally studied by injecting water through rectangular slot nozzles tangentially onto the underside of flat and curved surfaces in ambient air at atmospheric pressure. Although the film in Prometheus is injected into a near-vacuum, a simple force balance across an arbitrary control volume of fluid starting at the film free surface demonstrates that atmospheric pressure acts across the entire film (neglecting the small weight of the fluid inside the control volume). The forces due to atmospheric pressure balance across the film and can therefore be neglected.

Four different surfaces—glass, stainless steel, Plexiglas, and glass coated with a commercial product to make it "nonwetting," with varying surface wettability characterized by water-solid contact angles $\alpha_{LS} \approx$ 25 to 85 deg—were investigated. Both flat and curved surfaces with a radius of curvature $R = 5$ m were studied. The mean film detachment length downstream of the nozzle exit $x_d$ and the average film lateral extent $W$ at various downstream locations were measured for various values of initial film (i.e., nozzle) thickness $\delta$, initial film injection velocity $U$, and plate orientation with respect to the horizontal $\theta$. The important dimensionless groups in this flow are the Weber and Froude numbers, or We $= \rho_L U^2 \delta/\sigma$ and Fr $= U/\sqrt{g(\cos\theta)\delta}$, respectively. In these studies, $\delta = 1$ to 2 mm, $U = 1.9$ to 11 m/s, and $\theta = 0$ to 45 deg, giving We = 100 to 3200 and Fr = 15 to 120. In all cases, $\delta \geq 1$ mm and $U \geq 1$ m/s to prevent dry patch formation. Our results on film detachment and lateral spread are the first (to our knowledge) for turbulent liquid films on downward-facing flat and curved surfaces.

### III.A. Experimental Apparatus

Accurate numerical predictions of detachment and lateral spread in this free-surface turbulent flow are effectively impossible because of the prohibitive computational cost (at present) of simulating a moving interface in a turbulent flow and difficulties in determining appropriate boundary conditions for the meniscus formed near the detachment point. An experimental study was therefore conducted. As shown in Fig. 12, water is driven by a 0.5-hp centrifugal pump (Teel 2P39C) through a flexible coupling and then a flow straightening section and exits through a rectangular nozzle at an adjustable angle $\theta$ with respect to the horizontal. The water is injected by the nozzle tangentially onto the underside of either a flat or curved plate with a width of ~0.4 m extending a distance of 1.83 m downstream of the nozzle exit. The nozzle was mounted in a bracket designed

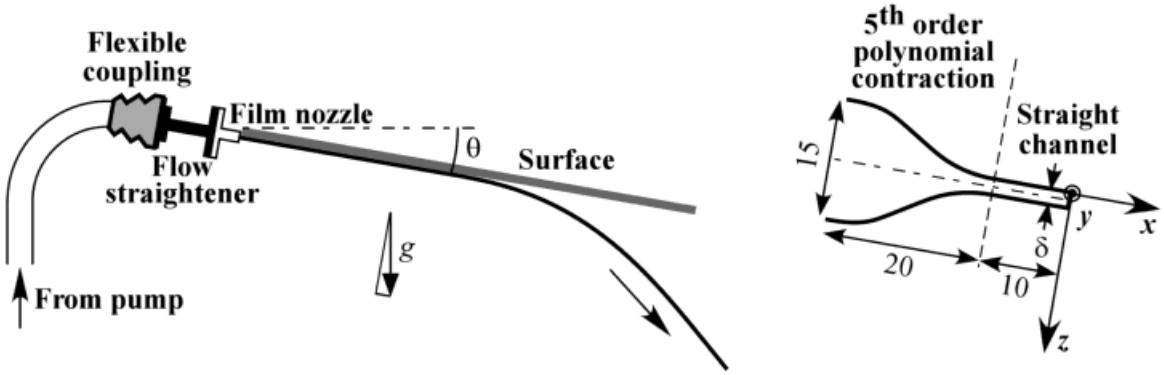


Fig. 12. Sketch of the flow loop [left] and film nozzles [right] for the forced film experiments. All dimensions are given in millimeters.

so that its vertical position and angular orientation about the $x$ and $y$ directions could be independently adjusted to ensure that the inner lip of the nozzle was flush with and parallel to the upstream end of the plate to ensure that the water would be injected tangential to the plate surface. The flow, which either detaches from the plate or hits a vertical splash guard at the downstream end of the plate, then falls into a 840-$\ell$ (220-gal) receiving tank below, where it is recirculated by the pump. The curvilinear coordinate system for this flow is defined as follows: $x$ along the (attached) flow direction and the plate surface, $y$ along the long dimension of the film or parallel to the plate surface, and $z$ downward along the short dimension of the film (i.e., thickness) or normal to the plate surface. Further details of the experiments are given by Anderson[26] and Shellabarger.[27]

Three different nozzles with a $z$ dimension at the exit $\delta = 1$, 1.5, and 2 mm and a $y$ dimension $W_o = 5$ cm (or aspect ratios $AR = 50$, 33, and 25, respectively) were fabricated using stereolithography rapid prototyping with a minimum fabrication tolerance of 0.1 mm (based upon the spatial resolution of the rapid prototyping machine). The nozzles were two-dimensional fifth-order polynomial contractions, followed by a straight channel at the exit, to produce uniform flow with thin boundary layers (see Fig. 12 right). The flow straightening section consisted of a perforated plate (53.6% open area ratio, 0.21-cm-diam staggered holes), followed by a 1.8-cm section of honeycomb (cell diameter 0.16 cm), both of stainless steel. The edge-to-edge spacing between the perforated plate and honeycomb, and the honeycomb and the nozzle inlet, were 7 and 50 mm, respectively.

The Prometheus study proposed using a molten lead film on the SiC first wall for thin liquid film protection. Since lead is essentially nonwetting on SiC surfaces, and little is known about the effect of surface wettability on the detachment and lateral spread of turbulent liquid films, experimental studies were also carried out on the effect of surface wettability on the film flow. Four different surfaces were studied:

1. glass (contact angle $\alpha_{LS} = 25$ deg)
2. stainless steel ($\alpha_{LS} = 50$ deg)
3. Plexiglas ($\alpha_{LS} = 75$ deg)
4. "nonwetting glass," or glass coated with a very thin-layer of Rain-X® (Pennzoil-Quaker State Company) ($\alpha_{LS} = 85$ deg).

The contact angle for all four surfaces was estimated by visual inspection of a 0.04-$\ell$ drop of water (illuminated by white light from above) on each surface.

In the Prometheus study, the large flow speeds tangential to the first wall over the hemispherical upper end cap of the reactor chamber generated a centrifugal force that helped to stabilize the film by keeping it attached to the first wall. For the flow speeds proposed for Prometheus of $U > 7$ m/s, the centrifugal acceleration $U^2/R$ (where the radius of curvature of the hemispherical end cap $R = 5$ m) easily exceeds that due to gravity $g$. Forced film flows were therefore investigated over flat plates of glass, stainless steel, Plexiglas, and nonwetting glass, and curved plates with $R = 5$ m about the $y$ axis of stainless steel and Plexiglas. The curved Plexiglas surface was formed by bolting a 183- × 40- × 0.56-cm ($x \times y \times z$) flexible Plexiglas plate along both its (183-cm dimension) edges to two identical concave wooden forms cut in the shape of an arc with a radius of curvature of 5 m. The wooden forms were braced at their upstream and downstream ends by crossbars to ensure consistent overall surface curvature. The curved stainless steel surface was formed by bolting a 183- × 40- × 0.064-cm ($x \times y \times z$) flexible stainless steel plate over the curved Plexiglas plate. Note that the surface angle of inclination $\theta$ for the curved surfaces was measured with respect to the tangent to the surface at the nozzle exit (i.e., the upstream end of the plate). The detachment length and the lateral extent of the film flow were then measured for water films flowing over all six surfaces.

The Prometheus-H study, which used 14 heavy-ion beams with a total energy of 7 MJ, proposed using the forced film concept over the upper end cap of the reactor chamber. Since then, the number of ignition beams proposed for various IFE power plant design concepts has steadily increased, with 72 heavy-ion beams proposed for an updated HYLIFE-II design[28] and 192 laser beams under construction for the National Ignition Facility.[29] With this large a number of ignition beams, penetrations through the first wall for beam ports will be required over most of the interior of the reactor cavity, including the upper end cap. Therefore, protecting these beam ports from the flowing thin liquid film represents an important design issue for this type of protection.

As an initial study of protective dams around beam port penetrations, cylindrical dams were placed on the underside of both the flat glass and curved Plexiglas plates with their leading edge at $x = 7.62$ cm. The dams were held in place by a permanent rare-earth magnet (Raytheon 62428D) on the upper side of the plate. Galvanized steel tubing with outer diameter $d = 25.4$ mm and thickness $t = 1.8$ to 76.2 mm and carbon steel shims with $d = 15.9$ to 25.4 mm and $t = 0.51$ to 2.36 mm were used.

### III.B. Flow Visualization

After contacting the plate surface, the film propagates some distance along the $x$ direction and then detaches at some distance downstream of the nozzle exit. The detachment length was measured by taking $x$-$z$ "side views" of the flow in which the detachment point is clearly visible, as shown in Fig. 13. The film detaches at slightly different $x$ locations across the lateral ($y$) extent of the film, especially for smaller values of $U$. In all cases, the detachment distance on each image was therefore taken

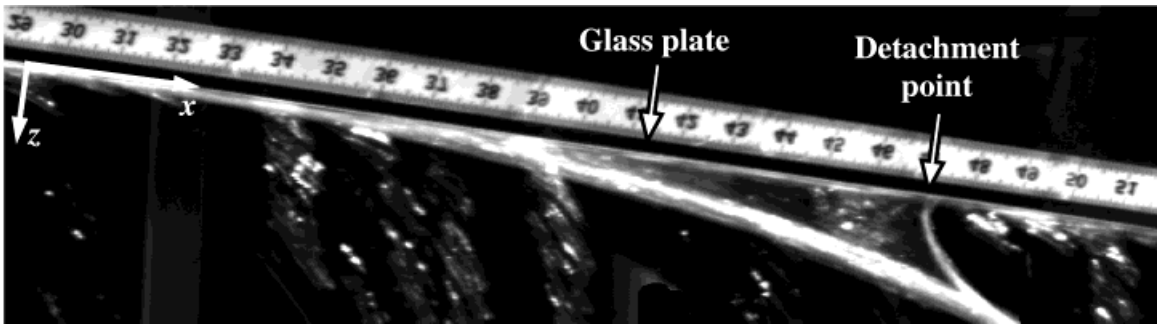


Fig. 13. Typical image showing detachment of the forced film from a flat glass surface at $\theta = 10$ deg for We = 1390 and Re = 9200. Note that the ruler above the glass plate is in inches.

to be the location farthest upstream (i.e., the smallest $x$ value) at which film detachment occurred.

Individual frames with an exposure of 8 ms were recorded at 30 Hz by a progressive scan monochrome charge-coupled-device camera (Pulnix TM-9701) onto the RAM of a personal computer using a framegrabber card (ImageNation PX610A) as 8-bit grayscale 640 column × 480 row images. Each individual image spans $7\tau$ to $90\tau$, where the flow convective timescale $\tau = \delta/U =$ 0.09 to 1.1 ms. A ruler or tape measure attached to the upper side of the plate was used to measure the detachment distance $x_d$ (in inches) along the plate surface for both flat and curved surfaces. Since the detachment distance can vary by up to ±2 cm between frames for this turbulent flow, the values reported here for mean detachment length $x_d$ are the average of 40 consecutive independent realizations obtained from images taken of the flow over a time period of 1.3 s.

For the glass and nonwetting glass surfaces, or the surfaces with the lowest and highest contact angles, respectively, the film width ($y$ extent) $W(x)$ was measured by visualizing the film through the top of the plate. In all cases, $W(x)$ varied by less than ±1 mm over time at any given downstream location $x$. Direct visual inspection was therefore used to measure $W(x)$ every 5 cm for $x < x_d$. Although drop formation was typically observed at the film free surface upstream of the detachment point, no dry patch formation was observed before detachment, as expected.

### III.C. Experimental Results

Figure 14 shows $x_d$ as a function of the Weber number We for the flat glass (○), stainless steel (□), Plexiglas (◇), and nonwetting glass (△) surfaces, all at $\theta = 0$ deg, for $\delta = 1$ mm (open), 1.5 mm (black), and 2 mm (gray) symbols. If no data are presented for a given case (usually for large We and $\theta$) in this and the subsequent graphs, detachment was not observed within the limits of the experimental apparatus (i.e., $x_d > 183$ cm). The detachment distance increases with Weber number and is smaller

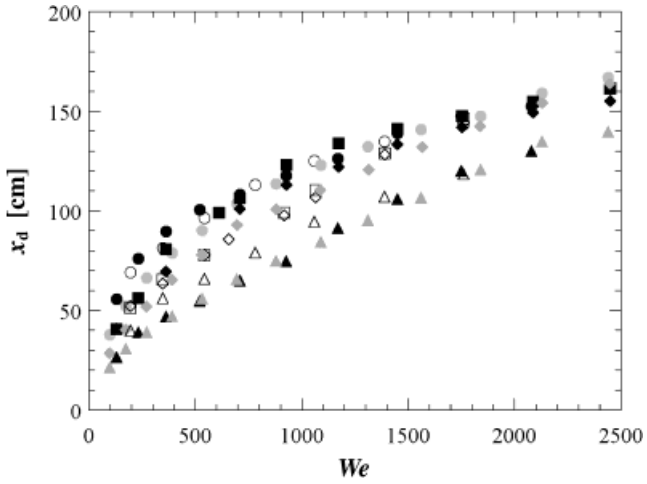


Fig. 14. Graph of $x_d$ as a function of We for flat glass (○), stainless steel (□), Plexiglas (◇), and nonwetting glass (△) surfaces at $\theta = 0$ deg and $\delta = 1$ mm (open), 1.5 mm (black), and 2 mm (gray) symbols.

for a more nonwetting surface (i.e., a surface with higher $\alpha_{LS}$) at a given We, demonstrating that surface wettability has a significant impact upon this flow. Moreover, $x_d$ is essentially independent of $\delta$ for a given We. The smallest or most conservative estimates of $x_d$ are hence for the most wetting glass surface.

Figure 15 shows $x_d$ versus We for the (a) flat glass and (b) nonwetting glass surfaces, or the surfaces with the lowest and highest contact angles, respectively. Data are shown for $\theta = 0$ deg (◇), 30 deg (△), and 45 deg (○) and $\delta = 1$ mm (open), 1.5 mm (black), and 2 mm (gray) symbols. Detachment length increases with $\theta$ for a given We, as expected since the component of gravity acting normal to the surface to detach the film decreases as $\theta$ increases. Although the data are not shown here, similar trends are observed for the two other surfaces.[27] The most conservative estimates of detachment are therefore for horizontal surfaces, or $\theta = 0$ deg.

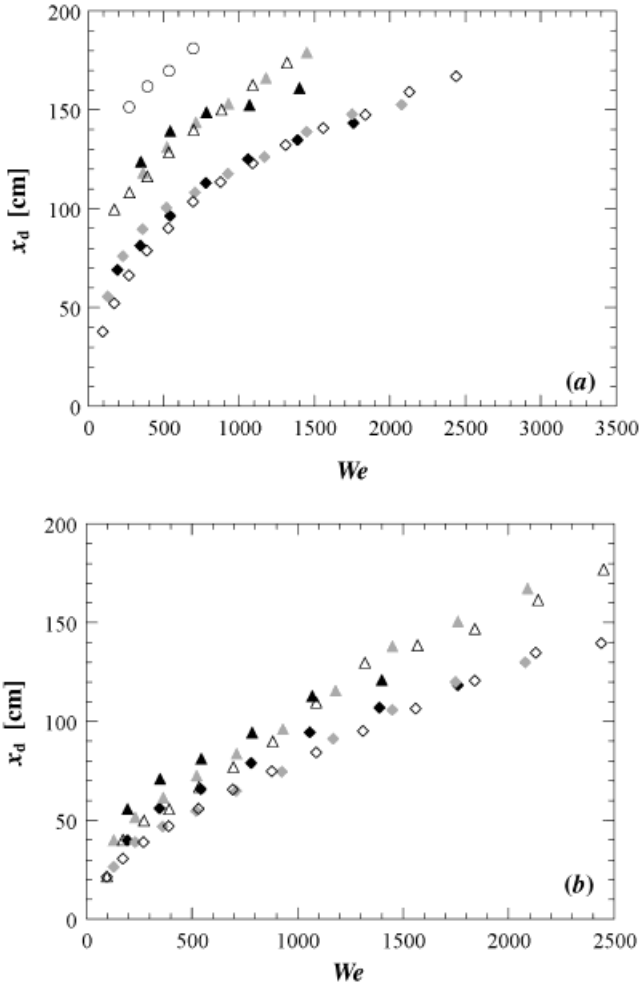


Fig. 15. Plot of $x_d$ versus We for (a) flat glass and (b) nonwetting glass surfaces at $\theta = 0$ deg (◇), 30 deg (△), and 45 deg (○) and $\delta = 1$ mm (open), 1.5 mm (black), and 2 mm (gray) symbols.

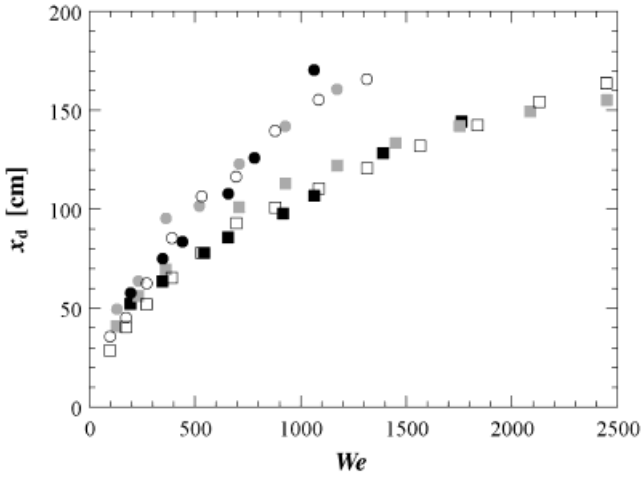


Fig. 16. Graph of $x_d$ as a function of We for flat (□) and curved Plexiglas (○) surfaces at $\theta = 0$ deg and $\delta = 1$ mm (open), 1.5 mm (black), and 2 mm (gray) symbols.

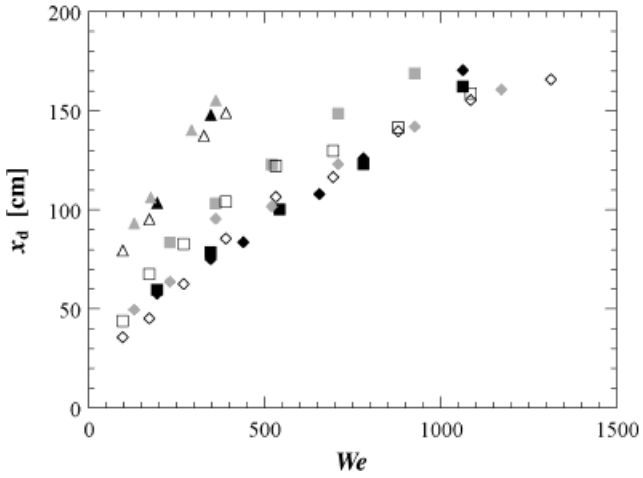


Fig. 17. Plot of $x_d$ versus We for the curved Plexiglas surface at $\theta = 0$ deg (◇), 10 deg (□), and 30 deg (△) for $\delta = 1$ mm (open), 1.5 mm (black), and 2 mm (gray) symbols.

Figure 16 shows $x_d$ versus We for the flat (□) and $R = 5$-m curved Plexiglas (○) surfaces at $\theta = 0$ deg and $\delta = 1$ mm (open), 1.5 mm (black), and 2 mm (gray) symbols. As expected, surface curvature stabilizes the film, delaying detachment and increasing $x_d$ by as much as 50%. Figure 17 shows $x_d$ versus We for the curved Plexiglas surface for $\delta = 1$ mm (open), 1.5 mm (black), and 2 mm (gray) symbols at $\theta = 0$ deg (◇), 10 deg (□), and 30° (△). As seen in Fig. 15 for the flat surfaces, $x_d$ increases with $\theta$ for a given We.

Figure 18 shows the normalized average detachment distance $x_d/\delta$ plotted as a function of Froude number Fr for the flat glass (○), stainless steel (□), Plexiglas (◇), and nonwetting glass (△) surfaces at $\theta = 0$ deg and $\delta = 1$ mm (open), 1.5 mm (black), and 2 mm (gray) symbols. The normalized detachment distance increases approximately linearly with Fr. As seen in Fig. 14, detachment occurs much closer to the nozzle (i.e., smaller $x_d$) for the relatively nonwetting (i.e., higher $\alpha_{LS}$) surfaces—Plexiglas and nonwetting glass. Edge effects due to nozzle geometry (characterized by $\delta$ for a constant nozzle $y$ dimension) appear to have almost no impact on the nonwetting glass surface data (△), probably because this surface "pins" the lateral edges, and hence fixes the $y$ extent, of the flow (see discussion of Fig. 19). The data also show that $x_d/\delta$ increases as $\delta$ decreases for all the values of $\theta$ studied. We hypothesize that this is due to a reduction in edge effects as $\delta$ decreases (for a constant nozzle $y$ extent) so that the flow would become more "two-dimensional."

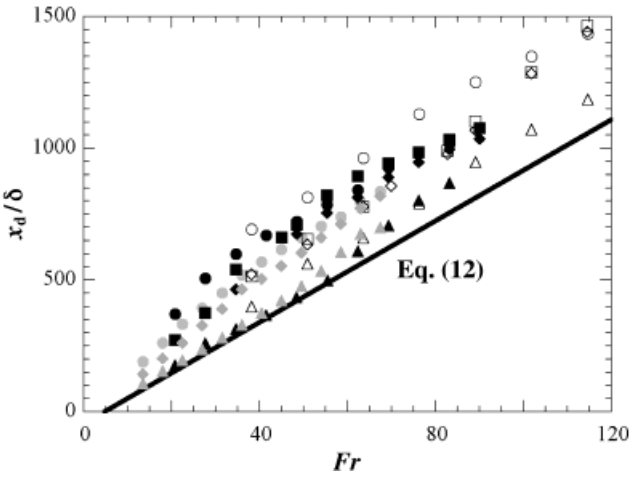


Fig. 18. Graph of $x_d/\delta$ as a function of Fr for flat glass (○), stainless steel (□), Plexiglas (◇), and nonwetting glass (△) surfaces at $\theta = 0$ deg and $\delta = 1$ mm (open), 1.5 mm (black), and 2 mm (gray) symbols. The solid line, given by Eq. (12), represents the lower bound on all these data obtained using a linear regression curve-fit.

Since these data at $\theta = 0$ deg have the smallest detachment lengths, the most conservative estimate for detachment length is then given by the solid line in Fig. 18, or

$$(x_d/\delta)_{min} = 11.56\text{Fr} - 16.1 \ . \qquad (12)$$

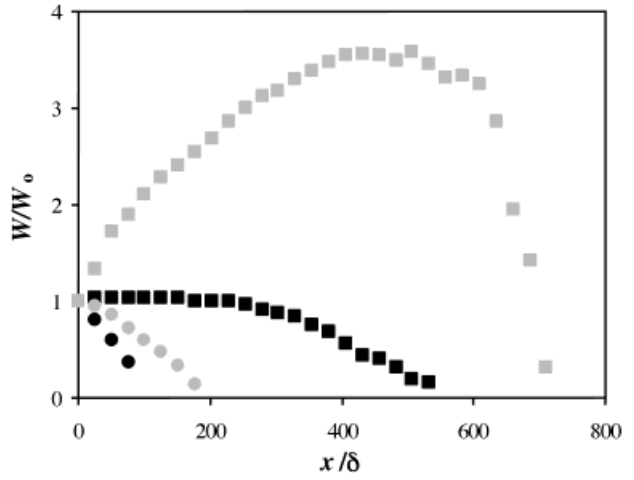


Fig. 19. Nondimensional film width $W/W_o$ as a function of normalized downstream distance $x/\delta$ for the wetting (gray) and nonwetting (black) symbols surfaces at $\theta = 0$ deg and $\delta = 2$ mm for We = 100 (○) and 1540 (□).

Equation (12) can be used by designers to predict the minimum spacing for injection slots for the forced film concept over both wetting and nonwetting surfaces.

The estimated errors in $x_d/\delta$ are 5, 6.8, and 10% for $\delta = 2$, 1.5, and 1 mm, respectively. The major source of error in these data is slight misalignments between the nozzle and the surface, along with variations in the initial film thickness $\delta$ due to fabrication tolerances. The maximum misalignment between the $y$ axis of the nozzle and the surface of the glass plate is 0.4 deg, resulting in a height difference of 0.4 mm, or 0.2 to 0.4$\delta$, across the 5-cm $y$ extent of the nozzle exit. The minimum geometric tolerance for the nozzles, based upon the spatial resolution of the rapid prototyping machine used to fabricate them, is 0.1 mm absolute, or 5 to 10% of $\delta$. The resultant variation in initial film thickness over the $y$ extent of the nozzle with respect to the glass surface due to these two factors can affect detachment distance and film width by introducing local variations in pressure gradient and flow speeds. We expect that errors due to local variations in the wettability of the various plate surfaces due to surface and water contamination are minimal since little variation was observed in either mean detachment length or film width over independent experimental runs under otherwise identical conditions.

Finally, Fig. 19 compares the average lateral ($y$) extent of the film normalized by its initial extent $W/W_o$ as a function of normalized downstream distance $x/\delta$ for the wetting (gray symbols) and nonwetting (black symbols) surfaces at $\theta = 0$ deg and $\delta = 2$ mm for We = 100 (○) and 1540 (□). The error in $W/W_o$ is estimated to be ±2% in all cases. The nonwetting surface has negligible lateral spread and contracts much more rapidly than the wetting surface. The nonwetting surface appears to fix, or "pin," the contact line for the film flow at the edges of the nozzle, thereby preventing the marked lateral growth of the flow observed for the wetting case. Numerical simulations of a three-dimensional wall jet, a flow similar to the forced film except that the injected and ambient fluids are identical, indicate that the remarkable lateral spread of these flows is due to the flow creating significant streamwise vorticity.[30] The lack of lateral spread for the nonwetting surface is therefore likely correlated to a decrease in streamwise vorticity in this flow.

The flow parameters proposed in Prometheus for the forced film over the upper part of the hemispherical end cap (where $\theta = 0$ to 45 deg) were We = 5900 to 190 000 and Fr = 100 to 680, versus the flow parameters range studied here of We = 100 to 3200 and Fr = 15 to 121. Moreover, the liquid lead films are nonwetting (i.e., have a contact angle of 90 deg) on the SiC walls proposed for Prometheus. These experimental data are therefore valid for the lower-speed (i.e., less turbulent) forced film cases, with the nonwetting glass and Plexiglas results being most relevant to the Prometheus design.

Equation (12), which gives a conservative estimate of film detachment over wetting or nonwetting surfaces,

suggests that the film may detach as soon as 0.46 m downstream of the injection slot (at Fr = 100 and $\delta$ = 0.5 mm). The upper end cap has a colatitudinal extent of 7.85 m. Although surface curvature may increase this value by as much as 50%, these results—and the excessive flow velocities required to reestablish the forced film between shots for a single injection slot—suggest that multiple injection slots (with corresponding regions downstream to remove the film fluid before it detaches) will be required to provide robust and complete coverage. The inner surface of the reactor chamber upper end cap may consist of several "tiles," or modular film injection/removal units. Moreover, the greater lateral contraction of these flows implies that injection slots must have significantly smaller longitudinal and colatitudinal spacing for nonwetting (versus wetting) surfaces. Both results indicate that forced film flows over curved wetting surfaces—which may require considering either alternative candidate coolant or first wall materials (or coating the SiC to create a wetting surface for liquid lead, as suggested in the Prometheus study)—with their marked lateral spread and greater detachment length, may be significantly more advantageous for IFE reactor chambers.

### III.D. Cylindrical Dams

Our experimental results for cylindrical dams to protect the beam ports showed that they were not compatible with the forced film concept. In all the cases studied here, the film either detached from either the flat glass or curved Plexiglas surface at the leading (upstream) edge (Fig. 20 top) or from the inside trailing edge of the obstruction (Fig. 20 center) and created a spray of drops falling into the "reactor cavity." In some cases, the film flowed smoothly over the entire obstruction, thus blocking the port (Fig. 20 bottom). Obviously, these are all unacceptable outcomes for effective forced film protection since a viable protective dam geometry requires that the film flow smoothly around (versus over) the dam, recover some distance downstream, and remain attached to the surface.

The APEX study has numerically simulated hydrodynamically shaped penetrations and backwall modifications to ensure that the film flow closes downstream of various penetration geometries.[10] We are therefore starting experiments on forced film flows around both streamlined dams and a scaled model of one of the elliptical penetrations with a linearly sloped and recessed backwall considered in the APEX study. This work will extend the results of the APEX study to film flows over shaped penetrations and backwalls with liquid-surface contact angles exceeding 0 deg.

These results suggest that designing penetration and backwall geometries that minimize disturbances to forced film flows may present a significant challenge to designers of IFE chambers utilizing the forced thin film wall protection concept. Alternatively, the driver beam array may be designed to avoid the reactor chamber upper end cap (difficult given the large number of beams in current IFE designs).

## IV. CONCLUSIONS

Over the last two years, numerical and experimental studies have been conducted on two types of thin liquid film protection, namely, the wetted wall and forced film concepts, as part of the ARIES-IFE study. These detailed investigations of the fluid dynamics aspects of these two concepts for protecting IFE reactor chamber first walls have identified several of the important design parameters for these concepts and identified the "design windows" for successful implementation of these concepts.

A numerical investigation has been performed to analyze the fluid dynamics aspects of the porous wetted wall protection scheme for IFE reactor first walls, focusing upon drop formation and detachment. The numerical results are in good agreement with initial experimental results. The model extends earlier work on the Rayleigh-Taylor instability by including the effect of a bounding wall through which the heavier fluid is continuously injected with mass transfer (evaporation/condensation) at the interface between the liquid film and chamber "gas." The results suggest that the stability of the liquid film

1. imposes a lower bound on the repetition rate in order to avoid liquid "dripping" into the reactor cavity between shots (Fig. 7)
2. imposes a lower bound on the liquid injection velocity in order to maintain the film thickness over the entire surface above some given minimum value to assure adequate wall protection from subsequent shots (Fig. 9).

The generalized charts presented in Figs. 7 and 9 make it possible for system designers to establish "design windows" for successful implementation of the wetted wall protection scheme with various coolants under a variety of operating conditions.

Experimental studies have been conducted on the hydrodynamics aspects of the forced film protection scheme for IFE reactor first walls, focusing upon film detachment, film lateral growth, and film flow around protective dams surrounding chamber penetrations typical of beam ports. The data confirm that surface wettability has a major impact upon the flow: The film detaches more closely to the injection point and has much less lateral growth over a nonwetting surface compared with a wetting surface. The experimental data are used to obtain a bounding relation [Eq. (12)] for conservative estimates of detachment length suitable for design purposes. The results imply the following:

1. A wetting chamber first wall surface is much more desirable from a design perspective, requiring far fewer injection slots than a nonwetting surface.

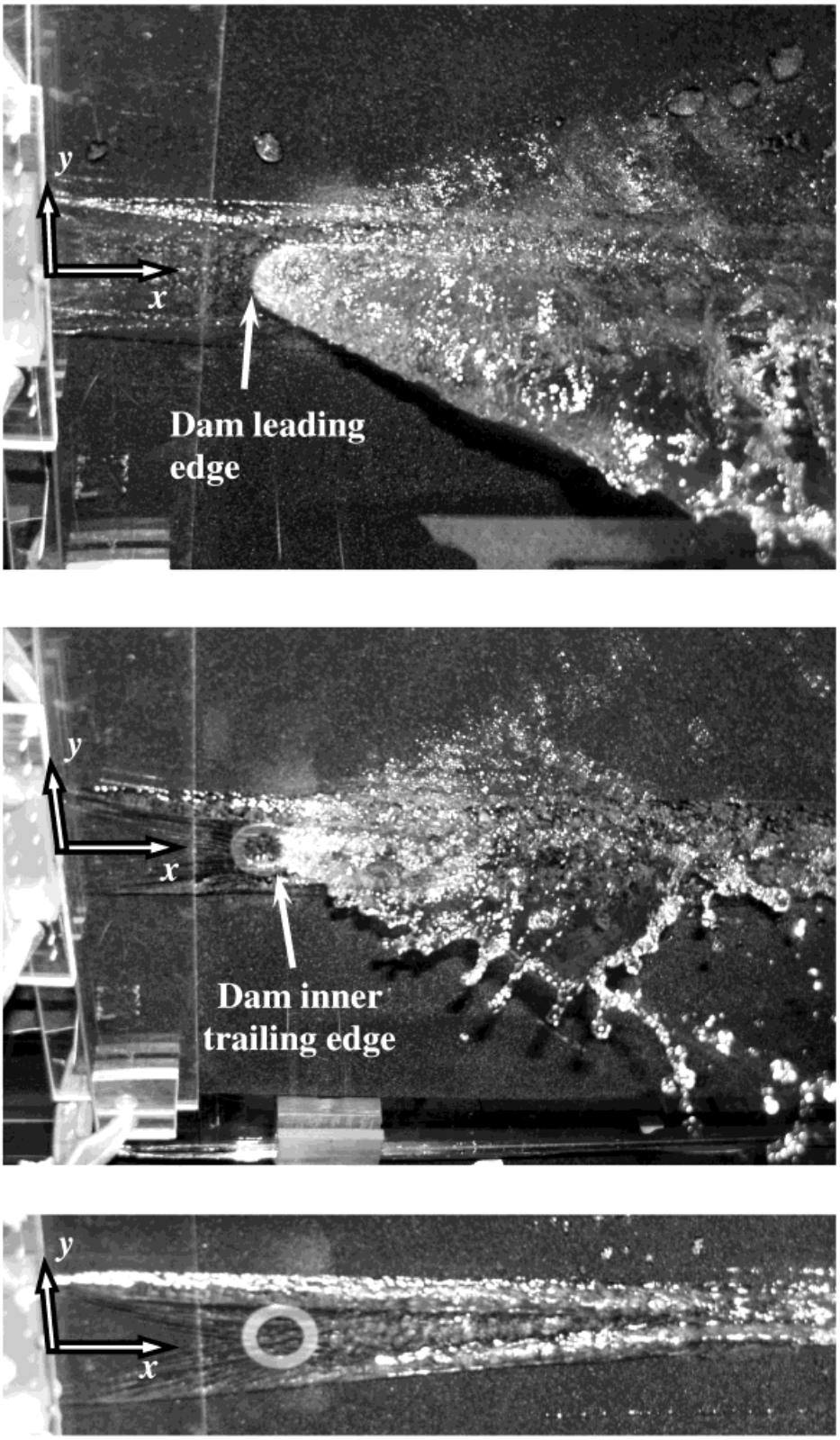


Fig. 20. Typical images of film detachment and spray formation at the cylindrical dam leading edge for $\delta = 1.5$ mm, We = 530, and $t = 2.36$ mm [top image]; film detachment and spray formation at the inner trailing edge for a similar case except that We = 200 [center image]; smooth film flow over the entire dam for $\delta = 1$ mm, We = 200, $t = 0.51$ mm [bottom image]. In all cases, $d = 25.4$ mm. These images are obtained from below the glass plate looking upward.

2. Cylindrical protective dams around chamber penetrations for beam or target injection appear to be incompatible with effective forced film protection.

Currently, experimental studies of various dam shapes (including those considered by the APEX study[10]) are being conducted to determine if there exist viable alternative protective dam geometries to shield the beam ports where the film separates around the dam and then recovers downstream of the dam, while remaining attached to the surface.

## ACKNOWLEDGMENTS

This research would not have been possible without the contributions of the other members of the Georgia Institute of Technology Fusion Engineering Group: F. F. Abdelall, J. K. Anderson, D. Juric, D. L. Sadowski, B. Shellabarger, and S. Shin. We wish to thank the ARIES-IFE Team for their suggestions and the U.S. Department of Energy Office of Fusion Energy Sciences for its support of this work through contract DE-FG02-01ER54656.

## REFERENCES

1. S. I. ABDEL-KHALIK and T. O. HUNTER, "Assessment of Surface Heating Problems in Laser Fusion Reactors," *J. Heat Transfer*, **100**, 311 (1978).

2. R. R. PETERSON, "Response of National Ignition Facility First Wall Materials to Target X-Rays and Debris," *Fusion Technol.*, **30**, 778 (1996).

3. P. F. PETERSON and J. M. SCOTT, "The Mini-Chamber, An Advanced Protection Concept for NIF," *Fusion Technol.*, **30**, 442 (1996).

4. A. HASSANEIN and I. K. KONKASHBAEV, *Modeling and Simulation of Fragmentation of Suddenly Heated Liquid Metal Jets*, ANL-ET/01-13, Argonne National Laboratory (2001).

5. R. R. PETERSON, D. A. HAYNES, Jr., I. E. GOLOVKIN, and G. A. MOSES, "Inertial Fusion Energy Target Output and Chamber Response: Calculations and Experiments," *Phys. Plasmas*, **9**, 2287 (2002).

6. G. L. KULCINSKI, R. R. PETERSON, L. J. WITTENBERG, E. A MOGAHED, and I. N. SVIATOSLAVSKY, "Dry Wall Issues for the SOMBRERO Laser Fusion Power Plant," *Fusion Eng. Des.*, **60**, 3 (2002).

7. L. M. WAGANER et al., "Inertial Fusion Energy Reactor Design Studies: Prometheus Final Report," MDC 92E0008 (DOE/ER-54101), Vol. III, U.S. Department of Energy (1992).

8. L. M. WAGANER, "Innovation Leads the Way to Attractive Inertial Fusion Energy Reactors—Prometheus-L and Prometheus-H," *Fusion Eng. Des.*, **25**, 125 (1994).

9. J. M. WILLIAMS et al., "A Conceptual Laser Controlled Thermonuclear Reactor Power Plant," *Proc. 1st Topl. Mtg. Technology of Controlled Fusion*, San Diego, California (1974).

10. M. A. ABDOU et al., "On the Exploration of Innovative Concepts for Fusion Chamber Technology," *Fusion Eng. Des.*, **54**, 181 (2001).

11. D. H. SHARP, "An Overview of Rayleigh-Taylor Instability," *Physica D*, **12**, 3 (1984).

12. G. TRYGGVASON and S. O. UNVERDI, "Computations of Three-Dimensional Rayleigh-Taylor Instability," *Phys. Fluids A*, **2**, 656 (1990).

13. A. ELGOWAINY and N. ASHGRIZ, "The Rayleigh-Taylor Instability of Viscous Fluid Layers," *Phys. Fluids*, **9**, 1635 (1997).

14. K. J. CHU and A. E. DUKLER, "Statistical Characteristics of Thin, Wavy Films. III. Structure of the Large Waves and Their Resistance to Gas Flow," *Am. Inst. Chem. Eng. J.*, **21**, 583 (1975).

15. G. J. GIMBUTIS, A. J. DROBAVICIUS, and S. S. SINKUNAS, "Heat Transfer of a Turbulent Water Film at Different Initial Flow Conditions and High Temperature Gradients," *Proc. 6th Int. Heat Transfer Conf.*, Toronto, Canada, Vol. 1, p. 321 (1978).

16. L.-Q. YU, F. K. WASDEN, A. E. DUKLER, and V. BALAKOTAIAH, "Nonlinear Evolution of Waves on Falling Films at High Reynolds Number," *Phys. Fluids*, **7**, 1886 (1995).

17. M. S. EL-GENK and H. H. SABER, "Minimum Thickness of a Flowing Down Liquid Film on a Vertical Surface," *Int. J. Heat Mass Transfer*, **44**, 2809 (2001).

18. Y. HASHIDATE, K. SHIODA, and S. NONAKA, "Experimental Study on the Flow Behavior of a Liquid Film on an Inclined Downward-Facing Plate," *Trans. Japan Soc. Mech. Eng. B*, **59**, 770 (1993) (in Japanese with English abstract).

19. S. SHIN, D. JURIC, and S. I. ABDEL-KHALIK, "Hydrodynamic Stability of the Porous Wetted Wall Protection Schemes in IFE Reactors," *Fusion Eng. Des.*, **65**, 611 (2003).

20. S. SHIN, F. ABDELALL, D. JURIC, S. I. ABDEL-KHALIK, M. YODA, D. SADOWSKI, and ARIES TEAM, "Fluid Dynamic Aspects of the Porous Wetted Wall Protection Scheme for IFE Reactors," *Fusion Sci. Technol.*, **43**, 366 (2003).

21. S. SHIN, S. I. ABDEL-KHALIK, D. JURIC, and M. YODA, "Effects of Surface Evaporation and Condensation on the Dynamics of Thin Liquid Films for the Porous Wetted Wall Protection Scheme in IFE Reactors," *Fusion Sci. Technol.*, **44**, 117 (2003).

22. J. K. ANDERSON, S. G. DURBIN, D. L. SADOWSKI, M. YODA, and S. I. ABDEL-KHALIK, "Experimental Studies of High-Speed Liquid Films over Downward-Facing Surfaces for IFE Wet Wall Concepts," *Fusion Sci. Technol.*, **43**, 401 (2003).

23. J. K. ANDERSON, M. YODA, S. I. ABDEL-KHALIK, and D. L. SADOWSKI, "Experiments on High-Speed Liquid Films over Downward-Facing Wetting and Nonwetting Surfaces," *Fusion Sci. Technol.*, **44**, 132 (2003).

24. S. O. UNVERDI and G. TRYGGVASON, "A Front-Tracking Method for Viscous, Incompressible, Multi-Fluid Flows," *J. Comput. Phys.*, **100**, 25 (1992).

25. S. SHIN, "A Level Contour Reconstruction Method for Three-Dimensional Multiphase Flows and Its Application," PhD Thesis, Georgia Institute of Technology (2002).

26. J. K. ANDERSON, "Experimental Studies of High-Speed Liquid Films over Downward-Facing Surfaces for IFE Applications," MS Thesis, Georgia Institute of Technology (2002).

27. B. T. SHELLABARGER, "Studies of Liquid Films on Downward-Facing Flat and Curved Surfaces," MS Thesis, Georgia Institute of Technology (2003).

28. J. F. LATKOWSKI and W. R. MEIER, "Heavy-Ion Fusion Final Focus Magnet Shielding Designs," *Fusion Sci. Technol.*, **39**, 798 (2001).

29. W. J. HOGAN, E. MOSES, B. WARNER, M. SOREM, J. SOURES, and J. HANDS, "The National Ignition Facility Project: An Update," *Fusion Sci. Technol.*, **39**, 329 (2001).

30. T. J. CRAFT and B. E. LAUNDER, "On the Spreading Mechanism of the Three-Dimensional Turbulent Wall Jet," *J. Fluid Mech.*, **435**, 305 (2001).